Whole genome CRISPR screening identifies TOP2B as a potential target for IMiD sensitization in multiple myeloma

Thalidomide analogues (IMiD), such as lenalidomide (LEN) and pomalidomide (POM) have significantly improved survival in patients with multiple myeloma (MM).[1] However, many patients relapse despite continued IMiD exposure, and IMiD-resistance remains a significant clinical problem. IMiD engage Cereblon (CRBN), an adaptor for the CUL4A-DDB1-RBX1 E3 ligase complex to promote proteasome-dependent degradation of neosubstrates IKZF1 (Ikaros) and IKZF3 (Aiolos). The degradation of these transcription factors is both directly toxic to MM cells and immunostimulatory to T cells.[2–4] Interrogation of the molecular events driving IMiD-mediated engagement of CRBN neosubstrates has greatly improved our mechanistic understanding of these agents. Acquired or intrinsic IMiD-resistance may occur through several mechanisms including loss of expression of CRBN and/or associated E3 ligase factors.[5,6] However, deeper insight into IMiD-resistance mechanisms may inform novel therapeutic approaches. Here, genome-wide CRISPR-Cas9 screening was employed to characterize resistance mechanisms and resensitization factors in isogenic IMiD-sensitive and -resistant MM lines. Loss of DNA topoisomerase IIβ (TOP2B) resensitized IMiD-refractory cells to IMiD and its inhibition with the cardio-

protective drug, dexrazoxane (DXZ), potentiated IMiD activity. Collectively, these findings identify TOP2B as a potential new therapeutic target in MM.

LEN-resistant MM1.S (MM.1Sres) cells were previously derived by culturing MM.1S cells in presence of increasing doses of LEN.[7] MM.1Sres cells displayed no significant increase in cell death upon prolonged (7 days) LEN exposure, while isogenic MM.1S cells were sensitive to LEN-induced cell death (Figure 1A). MM.1Sres cells also exhibited resistance to the anti-proliferative effects of LEN and POM as demonstrated by CellTrace Violet (CTV) labeling (Figure 1B). As previously reported,[7] MM.1Sres cells showed reduced CRBN expression and reduced IKZF3 degradation upon IMiD treatment as compared to MM.1S (Figure 1C).

In order to determine genes and pathways required for IMiD anti-myeloma activity in MM.1S cells, a genome-scale CRISPR knockout screen was performed in MM.1S-Cas9 cells treated with LEN, POM or dimethyl sulfoxide (DMSO) (Figure 1D). Genetic dependencies of MM.1S-Cas9 cells were identified by loss-of-representation of short guide RNA (sgRNA) in (DMSO)-treated cells and identified genes such as *MYC, IRF4, IKZF1* and *IKZF3* (*Online Supplementary Figure S1A*). MM.1S-Cas9 cells were dependent on essential processes such as RNA metabolism and DNA-damage related pathways (*Online Supplementary Figure S1B and C*). Deletion of CRBN and members of the COP9 signalosome (CSN), a 9-protein
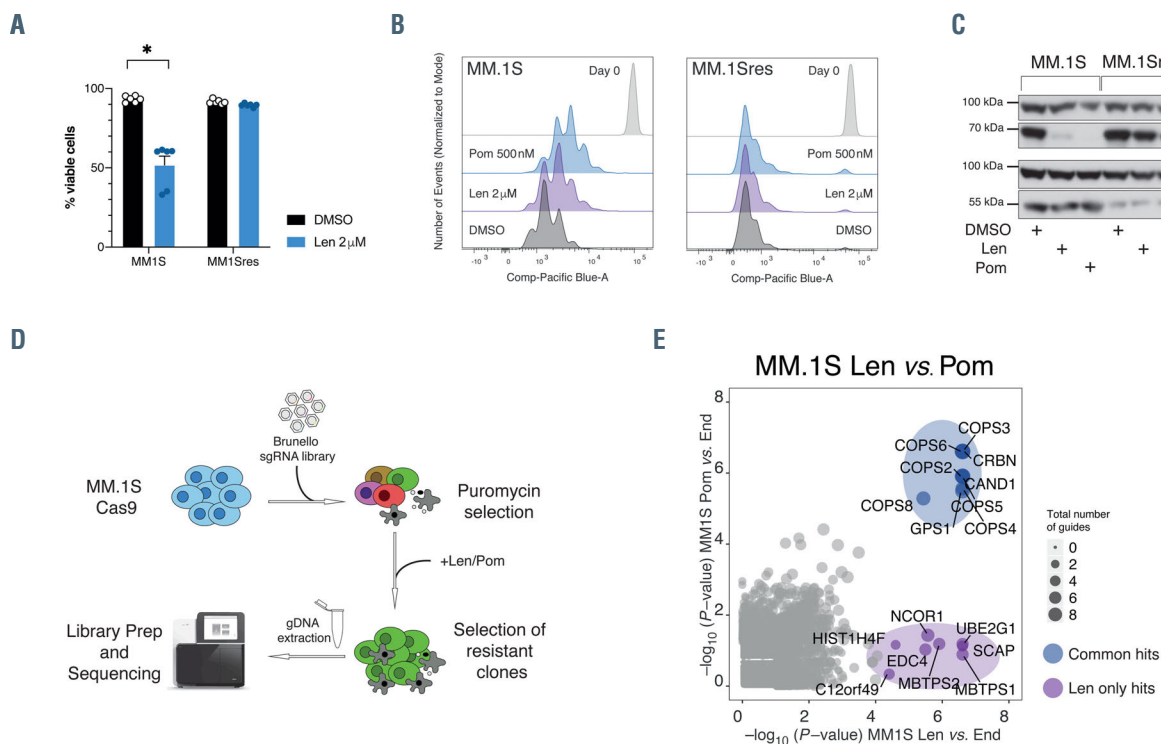

Figure 1. Resistance to lenalidomide and pomalidomide is mediated by loss of Cereblon and the COP9 signalosome. (A) Bar plot representing the percentage of propidium iodide negative (PI⁻, viable) MM.1S and lenlidomide (LEN)-resistant MM1.S (MM.1Sres) MM.1Sres cells treated with dimethyl sulfoxide (DMSO) or LEN (2 µM) for 7 days. Results are aggregated from n=3 independent experiments with two technical replicates per experiment. Error bars represents the mean ± standard error of the mean of the three biological replicates with their respective technical replicates; *P<0.0001. (B) CellTrace™ Violet/propidium iodide proliferation assay comparing proliferation of MM.1S and MM.1Sres cells in presence of LEN (2 µM) or pomalidomide (POM) (500 nM) (day 7 timepoint) in comparison to vehicle (DMSO). Results are representative of three independent experiments. (C) Immunoblot of IKZF3 and Cereblon (CRBN) levels in DMSO-, LEN- (2 µM) or POM- (500 nM) treated MM.1S and MM.1Sres cells for 16 hours (blots are representative of n=3 independent experiments). (D) Schematic representation of the CRISPR genome-scale resistance screen workflow. Approximately 500x10⁶ MM.1Sres-Cas9 cells were transduced with the Brunello genome-wide library, selected with puromycin and then treated with DMSO, LEN (2 µM) or POM (500 nM) for approximately 8 weeks. Genomic DNA was extracted for library preparation and Illumina sequencing. (E) Scatter plot showing hits overlapping between LEN and POM that are significant for adjusted P<0.05 and hits unique to LEN-treated cells significant for adjusted P<0.05.

complex involved in protein turnover regulation, were the most significantly enriched sgRNA in the presence of continued IMiD exposure (Figure 1E; *Online Supplementary Figure S1D to E*), validating previously published data.[5,6] Gene ontology (GO) analysis and protein-protein interaction (PPI) networking revealed that CSN may also modulate CUL4-DDB1 functions in response to DNA damage (*Online Supplementary Figure S1F and G*). Notably, some sgRNA (*NCOR1, EDC4, SCAP, UBE2G1, MBTPS1/2*) conferred selective resistance to LEN but not
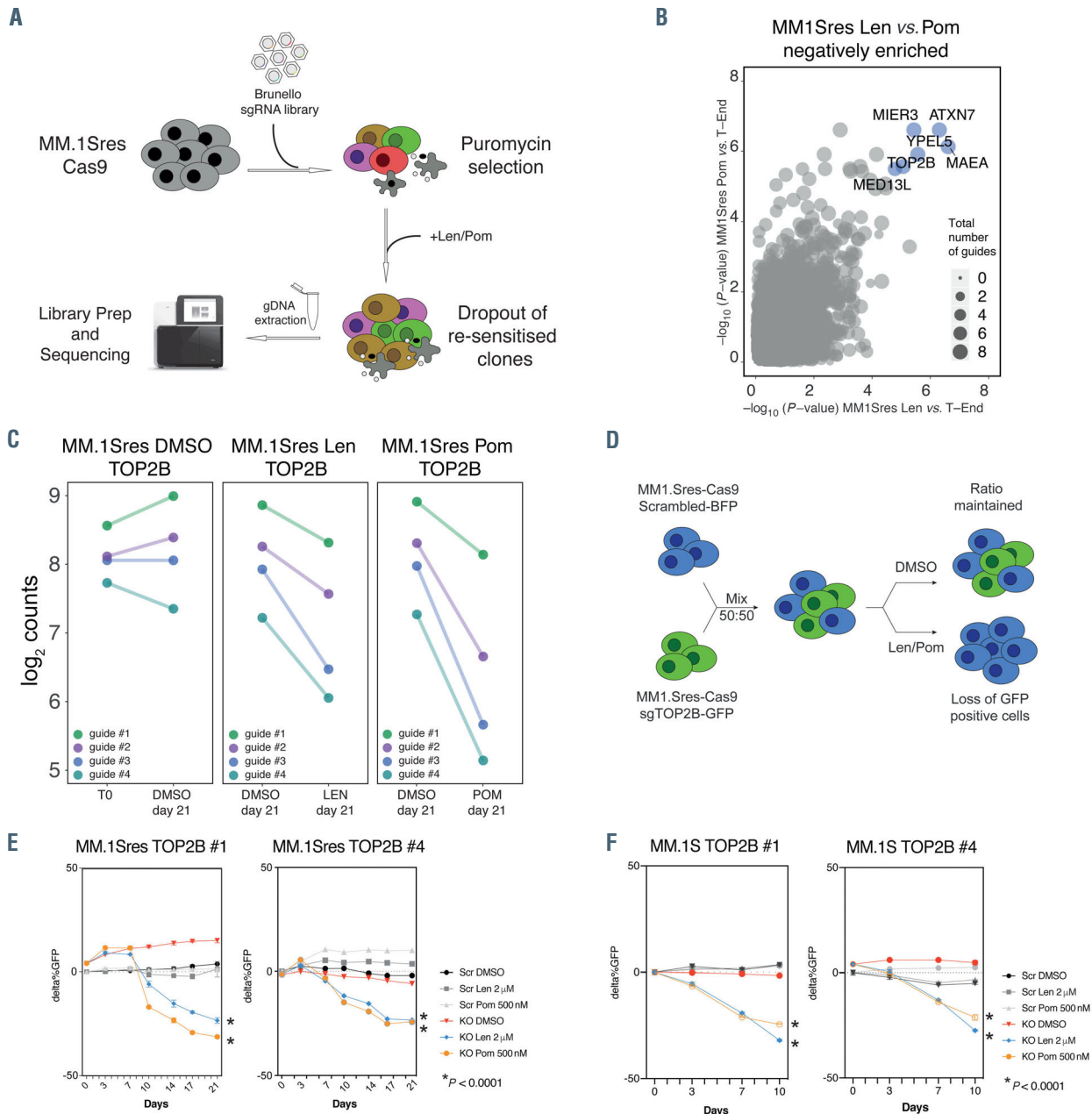

Figure 2. *TOP2B* deletion synergizes with Thalidomide analogues (IMiD) in MM.1S and MM.1S resistant cells. (A) Schematic representation of the CRISPR genome-scale dropout screen workflow. Approximately 500x10^{6} MM.1Sres-Cas9 cells were transduced with the Brunello genome-wide library, selected with puromycin and then treated with dimethyl sulfoxide (DMSO), lenalidomide (LEN) (2 μM) or pomalidomide (POM) (500 nM) for 3 weeks. Genomic DNA (gDNA) was extracted for library prepraration and Illumina sequencing. (B) Scatter plot overlapping the -log$_{10}$ (*P*-value) of negatively enriched guides in MM.1Sres-Cas9 cells treated with LEN and POM at the end of the screen. (C) Normalized counts (in log$_2$) at the end of the screen (T-End) of short guide RNA (sgRNA) specific for *TOP2B* in MM.1Sres. In the DMSO condition, the counts are compared to a timepoint zero (T-0) reference. In the LEN and POM conditions, the counts for sg*TOP2B* in T-End are plotted relatively to the average counts in the DMSO T-End condition. (D) Schematic representation of the competitive proliferation assay workflow. MM.1S- or MM.1Sres-Cas9 scramble-BFP cells were grown in competition with MM.1Sres-Cas9 sg*TOP2B*-GFP at a 1:1 ratio in DMSO, LEN (2 μM) or POM (500 nM) to validate the data observed in the genome-wide dropout screen. (E) Representative experiment of n=3 independent replicates showing the change in percentage of MM.1Sres-Cas9 sg*TOP2B*-GFP+ cells grown in competition with MM.1Sres-Cas9 Scramble-BFP+ cells treated with DMSO, LEN (2 μM) or POM (500 nM) for 21 days. Each dot with relative error bars represent the mean ± standard deviation of values from two technical replicates. (F) Representative experiment of three independent replicates showing the change in percentage of MM.1S-Cas9 scramble- or sgTOP2B-GFP+ cells grown in competition with MM.1S-Cas9 scramble-BFP+ cells (at a 1:1 ratio) treated with DMSO, LEN (2 μM) or POM (500 nM) for 10 days. Each dot with relative error bars represent the mean ± standard deviation of values from two technical replicates. GFP: green fluorescent protein.
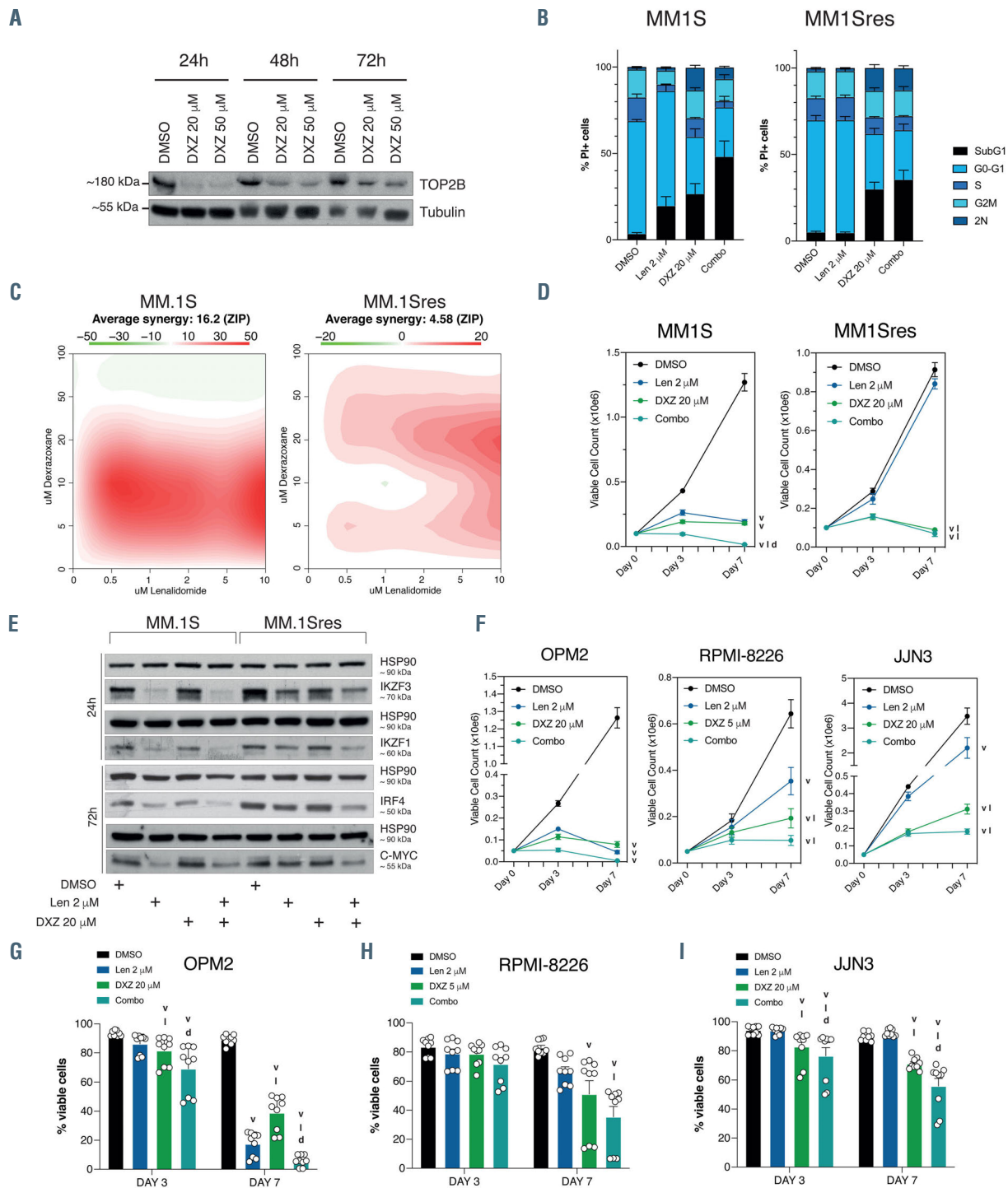
Figure 3. TOP2 inhibitor dexrazoxane displays anti-myeloma properties and combinatorial activity with lenalidomide. (A) Immunoblot showing TOP2B expression in MM.1S cells treated with dimethyl sulfoxide (DMSO) or dexrazoxane (DXZ) (20 μM or 50 μM) across 24, 48 and 72 hours. Tubulin expression is provided as a loading control. The experiment is representative of three biological replicates. (B) Bar graphs demonstrating Nicoletti cell cycle profiling of MM.1S and MM.1S resistant (MM1Sres) cells exposed to DMSO, lenalidomide (LEN) (2 μM), DXZ (20 μM) or combined LEN/DXZ (combo). The plot represents an aggregate of three independent experiments with three technical replicates each. Error bars represent mean ± standard error of the mean of n=3 independent experiments. v: significant *vs.* vehicle (DMSO); l: significant *vs.* LEN; d: significant *vs.* DXZ (*P*<0.05 or less). (C) Heatmaps representing the variation of zero interaction potency (ZIP) synergy score in MM.1S and MM.1Sres cells treated with increasing concentration of LEN and DXZ in combination. The average percentage of PI negative cells (viable) in each drug combination of three independent experiments was employed to compute synergy. The R package synergyfinder v2.2.4 was employed to perform the analysis. (D) Average viable cell count at 3 and 7 days for MM.1S and MM.1Sres treated with DMSO, LEN (2 μM), DXZ (5 μM or 20 μM depending on the cell line) or combined LEN/DXZ (combo). (E) Immunoblot showing expression of IKZF1, IKZF3 after 24h of treatment with DMSO, LEN (2 μM), DXZ (20 μM) or combined treatment and expression of IRF4 and MYC after 72 hours of treatment in the same conditions. HSP90 is provided as loading control. The experiment is representative of three biological replicates. (F) Viable cell count at 3 and 7 days of OPM2, RPMI-8226 and JJN3 cells treated with DMSO, LEN (2 μM), DXZ (20 μM) or combo. (G) Percentage of PI negative (viable) OPM2 cells treated with DMSO, LEN (2 μM), DXZ (20 μM) or combo and assessed by flow cytometry. (H) Percentage of PI negative (viable) RPMI-8226 cells treated with DMSO, LEN (2 μM), DXZ (5 μM) or combo and assessed by flow cytometry. (I) Percentage of PI negative (viable) JJN3 cells treated with DMSO, LEN (2 μM), DXZ (20 μM) or combo and assessed by flow cytometry. In (D), (F), (G), (H) and (I), error bars represent mean ± standard error of the mean of n=3 independent experiments. v: significant *vs.* vehicle (DMSO); l: significant *vs.* LEN; d: significant *vs.* DXZ (*P*<0.05 or less).

POM (Figure 1E), reflecting either a difference of potency and/or discrepant substrate specificity between the two IMiD.

The identification of genes that when deleted restore IMiD-sensitivity in MM.1Sres cells was achieved by a loss-of-representation CRISPR screen in 21-day LEN and POM-treated MM.1Sres-Cas9 cells relative to DMSO control (Figure 2A). The dependencies of DMSO-treated MM.1Sres-Cas9 cells partially overlapped and correlated with those of MM.1S-Cas9 cells, suggesting that acquired IMiD-resistance did not globally alter gene dependencies in these cells (*Online Supplementary Figure S2A to F*). In order to identify selective resentitization mechanisms in the presence of IMiD, the DMSO endpoint was compared with the matched timepoint in IMiD-treated MM.1Sres-Cas9 cells. This revealed that deletion of *ATXN7, TOP2B, MIER3, YPEL5, MAEA* and *MED13L* sensitized MM.1Sres cells to both LEN and POM (Figure 2B and C). *ATXN7* is part of the deubiquitination module of STAGA, a multisubunit entity involved in transcriptional regulation and DNA repair.[8] *MED13L* and *MIER3* also modulate transcription.[9,10] Interestingly, *YPEL5* and *MAEA* co-operate in an E3 ligase complex targeting gluconeogenesis enzymes.[11] However, *TOP2B* was selected for further study due to its potential tractability as a drug target. TOP2B is an enzyme which resolves topological DNA constraints during replication, transcription and repair.[12] In order to validate that *TOB2B* loss resensitizes to IMiD, competitive proliferation assays were performed in the presence and absence of LEN and POM (Figure 2D). MM.1Sres-Cas9 cells expressing two independent *TOP2B* sgRNA with a GFP reporter were mixed at a 1:1 ratio with MM.1Sres-Cas9 cells expressing a non-targeting sgRNA with a BFP reporter *(*Figure 2D to E; *Online Supplementary Figure S2G).* Consistent with the CRISPR-screen results, a competitive loss of GFP+ relative to BFP+ cells was observed following IMiD treatment (Figure 2E) confirming that *TOP2B* deletion confers IMiD-sensitivity in MM.1Sres-Cas9 cells. Analogous assays in MM.1S-Cas9 cells revealed that *TOP2B* loss further sensitized these cells to the anti-tumour effects of IMiD (Figure 2F), indicating that *TOP2B* deletion enhances IMiD activity in both IMiD-naïve and resistant contexts. *TOP2B* deletion had little or no effect on CRBN expression or subsequent IKZF3 degradation following IMiD treatment (*Online Supplementary Figure S3A and B*). MYC levels appeared to be modestly more downregulated in IMiD-treated MM.1Sres-Cas9 compared to MM.1S-Cas9 cells while the IMiD-induced downregulation of IRF4 was similar in MM.1Sres-Cas9 compared to MM.1S-Cas9 cells ((*Online Supplementary Figure S3C*). These observations indicate that the resensitization to IMiD treatment following deletion of *TOP2B* likely does not depend on further effects on the IKZF1/3-IRF4-MYC axis.

Having discovered the IMiD-sensitizing effects of genetic *TOP2B* depletion in MM.1Sres-Cas9 cells, orthogonal assays using DXZ, a chemical inhibitor of TOP2 that induces selective degradation of TOP2B protein, were used to validate this observation. DXZ also possesses iron-chelating activity and is Food and Drug Administration-approved for prevention of anthracycline-induced cardiotoxicity.[13] In order to investigate whether DXZ-mediated TOP2B degradation would phenocopy genetic deletion, MM.1Sres and MM.1S cells were treated with DXZ alone or in combination with LEN. TOP2B degradation in DXZ-treated MM.1S cells was evident 24 hours (hrs) after drug exposure and remained low in treated cells for up to 72 hrs (Figure 3A) at clinically relevant concentrations.[14] Cell cycle analysis

demonstrated that concentrations of DXZ sufficient to induce TOP2B degradation were cytostatic in MM.1S and MM.1Sres cells, with accumulation of cells in SubG1 and >2N, suggesting apoptosis-induction and failure of cytokinesis (Figure 3B; *Online Supplementary S3D to F*). Combinatorial effects of LEN and DXZ were observed in MM.1S and MM.1Sres cells with DXZ alone inducing cytostasis in MM.1Sres cells (Figure 3C and D). Similar to the effects observed following TOP2B deletion, DXZ did not modulate CRBN expression or alter IKZF3 degradation (*Online Supplementary Figure S3G*). However, an effect of the LEN and DXZ combination on cMYC, IKZF1, IKZF3 and IRF4 expression (Figure 3E) was evident. These findings may indicate that the effects of LEN and DXZ converge on the IRF4-MYC axis in MM.1Sres cells downstream or in parallel to canonical CRBN-neosubstrate interactions. Subsequently, DXZ combination treatments were performed in IMiD-sensitive OPM2 cells and IMiD-resistant RPMI-8226 and JJN3 MM cell lines (Figure 3D). In OPM2 cells, DXZ and LEN alone induced robust growth inhibition with a combinatorial effect observed following treatment with both agents (Figure 3F and G). DXZ induced death of RPMI-8226 and JJN3 cells, with mild additivity in the presence of LEN (Figure 3F, H and I).

CRISPR-based dissection of the genetic dependencies of MM.1S cells provided additional insight into IMiD biology and acquired IMiD resistance. Consistent with the initial description of MM.1Sres,[7] downregulation of CRBN expression and attenuation of neosubstrate degradation appears to be the major mechanism of IMiD resistance in these cells. Synthetic generation of IMiD resistance using gene deletion in MM.1S cells recapitulated prior studies identifying CRBN and elements of the CSN.[5,6] Gene ontology analysis of these hits revealed their importance in transcription-coupled nucleotide excision repair (TC-NER). Moreover, CUL4 and DDB1 have been demonstrated to participate with CSN in DNA repair pathways such as NER and TC-NER.[15] IMiD-sensitivity in MM.1Sres cells was rescued by knockout of *TOP2B*, a gene that modulates DNA repair, chromatin stability and gene expression.[12] However, LEN did not induce a DNA damage response or synergize with etoposide in MM.1Sres cells, suggesting that DNA damage induction is not the primary re-sensitization mechanism (*Online Supplemennetary Figure S3H and I*). Genetic deletion of *TOP2B* was not lethal to MM.1Sres cells, however these cells were sensitized to IMiD-induced death. This phenotype seemed to be independent of an increase in CRBN activity or expression changes within the IKZF1/3-IRF4-MYC axis. The biology underpinning re-sensitization of MM.1Sres cells to IMiD through loss of TOP2B remains to be defined.

DXZ had demonstrable anti-MM properties and additional activity in combination with LEN, especially in IMiD-sensitive cells. Since *TOP2B* deletion did not induce growth inhibition, the single-agent activity of DXZ may depend upon TOP2A inhibition rather than TOP2B degradation or through other effects. Deletion or depletion of TOP2A can have deleterious effects on the growth and/or survival of cancer cells (*Online Supplemnentary Figure S3J*) but we do not have evidence clearly demonstrating that the anti-MM activity of DXZ is through effects on TOP2A. Given that DXZ did not appear to demonstrably impinge on the IKZF1/3-IRF4-MYC axis, exactly how DXZ confers anti-MM activity, either alone or in combination with IMiD, remains unknown. The IC$_{50}$ of DXZ across the MM lines tested spanned from 5 to 20 μM (data not shown), which is significantly lower than the peak plasma concentration

reached after a cardioprotective 500 mg/m^2 dose (36.5 μg/mL or 135 μM).[14] This suggests that DXZ could be repurposed as a TOP2-targeting anti-MM agent as part of a combinatorial approach, however its posology is not well suited to recurrent or chronic administration. We are unaware of any other selective small-molecule TOP2B inhibitors. Greater understanding of the structure-activity relationship between DXZ and TOP2B may allow the rational development of related chemotypes for drug therapy. Further investigation of these mechanisms by which TOP2B inhibition leads to anti-MM activity could reveal alternative pathways to IMiD potentiation.

Matteo Costacurta,[1,2] Stephin J Vervoort,[1,2] Simon J Hogg,[1,2] Benjamin P Martin,[1,2] Ricky W Johnstone[1,2#] and Jake Shortt[1,2,3,4#]

[1]Translational Hematology Program, Peter MacCallum Cancer Center, Melbourne; [2]Peter MacCallum Department of Oncology, The University of Melbourne, Parkville, Melbourne; [3]Monash Hematology, Monash Health, Clayton, Melbourne and [4]Blood Cancer Therapeutics Laboratory, School of Clinical Sciences at Monash Health, Monash University, Clayton, Melbourne, Victoria, Australia.

#RWJ and JS contributed equally as co-senior authors.

Correspondence:
RICKY W. JOHNSTONE - ricky.johnstone@petermac.org
JAKE SHORTT - jake.shortt@monash.edu
doi:10.3324/haematol.2020.265611

References

1. Kumar SK, Rajkumar SV, Dispenzieri A, et al. Improved survival in multiple myeloma and the impact of novel therapies. Blood. 2008;111(5):2516-2520.
2. Lu G, Middleton RE, Sun H, et al. The myeloma drug lenalidomide promotes the Cereblon-dependent destruction of Ikaros proteins. Science. 2014;343(6168):305-309.
3. Licht JD, Shortt J, Johnstone R. From anecdote to targeted therapy: the curious case of thalidomide in multiple myeloma. Cancer Cell. 2014;25(1):9-11.
4. Krönke J, Udeshi ND, Narla A, et al. Lenalidomide causes selective degradation of IKZF1 and IKZF3 in multiple myeloma cells. Science. 2014;343(6168):301-305.
5. Liu J, Song T, Zhou W, et al. A genome-scale CRISPR-Cas9 screening in myeloma cells identifies regulators of immunomodulatory drug sensitivity. Leukemia. 2019;33(1):171-180.
6. Sievers QL, Gasser JA, Cowley GS, Fischer ES, Ebert BL. Genome-wide screen identifies cullin-RING ligase machinery required for lenalidomide-dependent CRL4CRBN activity. Blood. 2018;132(12):1293-1303.
7. Zhu YX, Braggio E, Shi C-X, et al. Cereblon expression is required for the antimyeloma activity of lenalidomide and pomalidomide. Blood. 2011;118(18):4771-4779.
8. Ramachandran S, Haddad D, Li C, et al. The SAGA deubiquitination module promotes DNA repair and class switch recombination through ATM and DNAPK-mediated H2AX formation. Cell Rep. 2016;15(7):1554-1565.
9. Poss ZC, Ebmeier CC, Taatjes DJ. The Mediator complex and transcription regulation. Crit Rev Biochem Mol Biol. 2013;48(6):575-608.
10. Derwish R, Paterno GD, Gillespie LL. Differential HDAC1 and 2 recruitment by members of the MIER family. PLoS One 2017;12(1):e0169338.
11. Lampert F, Stafa D, Goga A, et al. The multi-subunit GID/CTLH E3 ligase promotes proliferation and targets the transcription factor Hbp1 for degradation. eLife. 2018;7e35528.
12. Chen SH, Chan N-L, Hsieh T. New mechanistic and functional insights into DNA topoisomerases. Biochemistry. 2013;82(1):139-170.
13. Lyu YL, Kerrigan JE, Lin C-P, et al. Topoisomerase II mediated DNA double-strand breaks: implications in doxorubicin cardiotoxicity and prevention by dexrazoxane. Cancer Res. 2007;67(18):8839-8846.
14. Brier ME, Gaylor SK, McGovren JP, Glue P, Fang A, Aronoff GR. Pharmacokinetics of dexrazoxane in subjects with impaired kidney function. J Clin Pharmacol. 2011;51(5):731-738.
15. Fischer ES, Scrima A, Böhm K, et al. The molecular basis of CRL4DDB2/CSA ubiquitin ligase architecture, targeting, and activation. Cell. 2011;147(5):1024-1039.